OXFORD

ORIGINAL ARTICLE

The Hyperpolarization-Activated HCN4 Channel is Important for Proper Maintenance of Oscillatory Activity in the Thalamocortical System

Mehrnoush Zobeiri[1], Rahul Chaudhary[1], Anne Blaich[2], Matthias Rottmann[1], Stefan Herrmann[2], Patrick Meuth[3], Pawan Bista[1], Tatyana Kanyshkova[1], Annika Lüttjohann[1], Venu Narayanan[3], Petra Hundehege[3], Sven G. Meuth[3], Maria Novella Romanelli[4], Francisco J. Urbano[5], Hans-Christian Pape[1], Thomas Budde[1] and Andreas Ludwig[2]

[1]Institut für Physiologie I, Westfälische Wilhelms-Universität, 48149 Münster, Germany, [2]Institut für Experimentelle und Klinische Pharmakologie und Toxikologie, Friedrich-Alexander-Universität Erlangen-Nürnberg, 91054 Erlangen, Germany, [3]Klinik für Neurologie mit Institut für Translationale Neurologie, Westfälische Wilhelms-Universität, 48149 Münster, Germany, [4]Department of Neurosciences, Psychology, Drug Research and Child Health, University of Florence, Via Ugo Schiff 6, 50019 Sesto Fiorentino, Italy and [5]IFIBYNE, CONICET, Universidad de Buenos Aires, Buenos Aires, Argentina

Address correspondence to Prof. Andreas Ludwig, Institut für Experimentelle und Klinische Pharmakologie und Toxikologie, Friedrich-Alexander-Universität Erlangen-Nürnberg, Fahrstr. 17, D-91054 Erlangen, Germany. Email: Andreas.Ludwig@fau.de/Prof. Thomas Budde, Westfälische Wilhelms-Universität, Institut für Physiologie I, Robert-Koch-Str. 27a, D-48149 Münster, Germany. Email: tbudde@uni-muenster.de

Mehrnoush Zobeiri, Rahul Chaudhary, Anne Blaich, Thomas Budde and Andreas Ludwig contributed equally

Abstract

Hyperpolarization-activated cation channels are involved, among other functions, in learning and memory, control of synaptic transmission and epileptogenesis. The importance of the HCN1 and HCN2 isoforms for brain function has been demonstrated, while the role of HCN4, the third major neuronal HCN subunit, is not known. Here we show that HCN4 is essential for oscillatory activity in the thalamocortical (TC) network. HCN4 is selectively expressed in various thalamic nuclei, excluding the thalamic reticular nucleus. HCN4-deficient TC neurons revealed a massive reduction of I_h and strongly reduced intrinsic burst firing, whereas the current was normal in cortical pyramidal neurons. In addition, evoked bursting in a thalamic slice preparation was strongly reduced in the mutant mice probes. HCN4-deficiency also significantly slowed down thalamic and cortical oscillations during active wakefulness. Taken together, these results establish that thalamic HCN4 channels are essential for the production of rhythmic intrathalamic oscillations and determine regular TC oscillatory activity during alert states.

Key words: HCN4 channels, HCN4 knock out mice, I_h, thalamocortical dysrhythmia, thalamocortical oscillations

Introduction

The 4 hyperpolarization-activated and cyclic nucleotide-gated channels HCN1–HCN4 underlie the I_h current in the nervous system (Ludwig et al. 1998; Kaupp and Seifert 2001; Robinson and Siegelbaum 2003; Biel et al. 2009). HCN1, HCN2, and HCN4 are the main isoforms in the brain, whereas HCN3 is expressed at lower levels (Moosmang et al. 1999; Monteggia et al. 2000; Santoro et al. 2000; Notomi and Shigemoto 2004). The function of HCN subunits in the brain has been examined by analyzing mutant mice. Lack of HCN1 leads to a motor defect as well as enhanced memory (Nolan et al. 2003, 2004) and increased susceptibility to a variety of genetically determined spontaneous and induced seizures (Strauss et al. 2004; Kole et al. 2007; Blumenfeld et al. 2008; Huang et al. 2009; Santoro et al. 2010). HCN2-deficient mice display ataxia and frequent absence seizures (Ludwig et al. 2003; Chung et al. 2009).

In contrast to the well-studied isoforms HCN1 and HCN2, direct evidence regarding the role of HCN4 in the brain is lacking. Since the global deficiency of HCN4 is an embryonic lethal mutation (Stieber et al. 2003), we generated a brain-specific deletion of this isoform. Utilizing this mouse model, we were able to identify a specific function of HCN4, which is different from that of the other HCN isoforms. We demonstrate that HCN4 accounts for the majority of I_h in thalamocortical (TC) neurons and controls the firing activity of these cells. Importantly, I_h was normal in mutant cortical pyramidal neurons. HCN4 knockouts did not show spontaneous absence seizures. Evoked bursting in a thalamic slice preparation was strongly reduced. In addition, we found that HCN4-deficiency slowed down thalamic and cortical oscillatory activity in the alert state. These results define a functional role for HCN4; we propose that the isoform is important in the maintenance and regulation of oscillatory activity in the TC system.

Materials and Methods

Mice

HCN4[+/L1] (Stieber et al. 2003) and Nestin-Cre (Tronche et al. 1999) were backcrossed to a C57BL/6 background for 8 generations and then crossed to obtain double heterozygotes (HCN4[+/L1], Nestin-Cre[tg/0]). These were mated with homozygous floxed HCN4 (HCN4[L2/L2]) (Stieber et al. 2003) to generate a brain-specific deletion (HCN4[L2/L1], Nestin-Cre[tg/0]). Controls were litter-matched HCN4[L2/+], Nestin-Cre[0/0]. For behavioral studies female mice were used; all other experiments were done by using males and females. All behavioral and electrophysiological analyzes were performed and evaluated blind with respect to genotype. All animal studies were performed in compliance with EU and national regulations for animal experimentation and have been approved by the 2 competent authorities Landesamt für Natur, Umwelt und Verbraucherschutz Nordrhein-Westfalen and Regierung von Mittelfranken, Germany.

Western Blotting

Dissected brain regions were frozen in liquid nitrogen, pulverized and boiled in 2% SDS, 50 mM Tris, pH 7.4 for 15 min. Western blotting was done as described (Ludwig et al. 1997). Blots were probed with rabbit polyclonal antibodies against HCN1 (Alomone Labs), HCN2 (Ludwig et al. 2003) and HCN4 (Alomone Labs). Labeling of MAP kinase with a p44/42 MAP kinase antibody (Cell Signaling Technology) served as loading control.

Quantitative RT-PCR

Total RNA was extracted with Trizol reagent. First-strand cDNA was primed with random hexamer primers and synthesized using Invitrogen SuperScript™ III and Fermentas RevertAid™ kit at 37° C for 60 min. The following hybridization primer/probe assays were used (Applied Biosystems): β_2-microglobulin, Mm00438887_m1; HCN1, Mm00468832_m1; HCN2, Mm00468538_m1, HCN3, Mm01212852_m1, HCN4, Mm01176086_m1. PCR was performed using the DyNAmo Flash Mastermix (Biozym) with the following program: 10 min at 95° C, 45 cycles: 15 s at 95 ° C and 1 min at 60 °C. CT values of HCN isoforms were normalized to β_2-microglobulin according to $\Delta CT = CT(HCN\ isoform) - CT(\beta_2\text{-microglobulin})$. ΔCT values were transformed into AU values by applying the formula $2^{-\Delta Ct} \times 100$.

Immunostaining

Brains were cut at –16 °C in 10 µm sections, fixed in 4% paraformaldehyde for 15 min and blocked with 10% normal goat serum. The primary antibody was polyclonal anti-HCN4 (Alomone Labs) diluted 1:200 in PBS, 0.01% Triton X-100. Bound antibodies were detected by the avidin–biotin-complex method using either peroxidase/3, 3′-diaminobenzidine or alkaline phosphatase/blue alkaline phosphatase substrate (Vector Laboratories) followed by counterstaining with Nuclear Fast Red. Antibodies used for double-label immunofluorescence analysis were polyclonal rabbit anti-HCN4 (1:200, Alomone Labs) and monoclonal mouse anti-NeuN conjugated with Alexa Fluor-488 (1:100, Santa Cruz Biotechnology). Brain slices were incubated with the antibodies diluted in 3% BSA in PBS and in the case of anti-HCN4 followed by incubation with an antirabbit Cy3 secondary antibody. Fluorescence images were captured with a LSM 5 Pascal microscope (Zeiss) and analyzed with Image-Pro Express (Media Cybernetics). Knockout and control slices were processed in parallel and images were acquired using identical settings.

EEG Telemetry

A telemetric system (Data Sciences) was used to assess potential pathological brain activity. Transmitters were implanted for EEG recording in freely moving animals according to a modification of a procedure described previously (Weiergraber et al. 2005). Male mice ($n = 7/9$ KO and control animals; age 3–5 months) were anesthetized by an i.p. injection (2.5 mL/kg BW) of 2.5 mg/mL ketamine, 2.3 mg/mL xylazine and 0.25 mg/mL acepromazine. The skin over the frontal skull was opened and a subcutaneous pouch at the lateral back was prepared using a blunt probe. The TA10TA-F20 transmitter was placed in the pouch and the 2 leads were tunneled subcutaneously to the cranium. After fixing the head in a stereotaxic apparatus (Narishige), 2 holes (~1.5 mm in diameter) were drilled in the skull 1 mm caudal and 1 mm lateral right and left of the bregma. The tips of the leads were exposed by stripping approximately 4 mm of the insulation and wires were placed in the skull holes. Electrodes were sealed in the holes with a small amount of acrylic cement (Kent Dental) and the incision was closed using 4-0 nonabsorbable sutures (Ethilon II, Johnson & Johnson). Mice were allowed to recover for at least 2 weeks. EEGs were recorded continuously for 24 h during a 12 h/12 h light–dark cycle. Data were analyzed using the Dataquest ART software (Data Sciences).

Local Field Potential Recordings

The 3–5 months old male HCN4-KO and control mice ($n = 3/7$ KO and WT mice) were used. Animals were anesthetized with

an i.p injection of 50 mg/kg pentobarbital supplemented by a subcutaneous injection of carprofen (5 mg/kg BW). Head was fixed in a stereotactic frame (David Kopf Instruments, USA) and holes were drilled into the skull on top of the right hemisphere for the insertion of isolated (except at the tip) stainless steel wire recording electrodes (diameter 0.127 mm; impedance 500 KΩ, Franco Corradi, Milan, Italy) in somatosensory cortex (SSC; A/P = 0, M/L = 3, depth = −1.2) and ventral–posterior medial nucleus of the thalamus (VPM; A/P = −1.7, M/L = 1.5, depth = −2.8). Two epidural silver wires placed on top of the cerebellum served as grounding and reference electrodes. The electrode assembly was fixed to the skull with the aid of dental acrylic cement. Following surgery, mice were allowed to recover for at least 1 week. Differential LFP signals (cortex to reference and thalamus to reference) were recorded continuously for 8 h during the light phase of the 12 h/12 h light-dark cycle (with lights on at 8 am). Recordings were performed in plexiglas registration boxes (30 × 20 × 20 cm³). Animals were connected to the recording set up via a cable and swivel allowing them to move freely during the recording. The LFP signals were amplified (Science Products DPA-2 F), filtered by a band pass filter with cut-off points at 1 (high pass) and 100 (low pass) and digitalized with a constant sample rate of 2 kHz by a CED recording-system (Cambridge Electronic Design, UK). The behavioral activity of the animals was registered by a Passive Infrared Registration System (PIR, LuNAR PR Ceiling Mount, Rokonet RISCO Group S.A., Belgium) placed on top of the registration box (van Luijtelaar et al. 2012). Following the LPF recordings animals were deeply anesthetized using isoflurane and brains were removed for histological verification of the correct electrode position. The offline analysis of the recordings was carried out using NeuroExplorer 4 (Nex Technologies, USA) and Spike2 (version 7.08, Cambridge Electronic Design, UK) software. The LFP data selection and analysis were performed as described before (Zobeiri, Chaudhary et al. 2018). Briefly, LFP data from SSC and VPM from 20 epochs of 10 s of active-wakefulness and deep slow-wave sleep were selected for each animal based on the LFP and PIR activity according to a commonly used criteria (van Luijtelaar et al. 2012; Zobeiri, Chaudhary et al. 2018; Zobeiri, van Luijtelaar et al. 2018). Only the first 2 h of the light period (high amount of deep non-REM sleep (Huber et al. 2000)) were selected for the analysis. Slow-wave sleep criteria: high-amplitude cortical LFP together with slow (1–4 Hz) waves in a motionless animal (low amplitude stable regular PIR signal). Active-wakefulness criteria: behavioral activity (high and variable PIR signal accompanied by low amplitude cortical LFP with theta and or beta waves). The power spectral density (PSD) of the signal was calculated for each individual animal, averaging the data from 20 epochs of 10 s duration each, for both active-wakefulness and slow-wave sleep separately. The power density of the peak frequency of the conventional frequency bands (delta: 1–4 Hz, theta: 4.5–8 Hz, alpha: 8.5–11, and beta: 11.5–30) was used for statistical analysis. To control for individual differences in EEG amplitude and PSD, relative values (Z-transformed) and percentages were analyzed.

Slice Preparation for Electrophysiological Recordings

Mice (P18–P30) were sacrificed and after surgically removing a skull cap caudal to the bregma, a block of brain tissue containing thalamus and cortex was removed from the cranial vault and submerged in ice-cold aerated (O_2) saline containing (in mM): sucrose, 200; PIPES, 20; KCl, 2.5; NaH_2PO_4, 1.25; $MgSO_4$, 10;

$CaCl_2$, 0.5; glucose, 10; pH 7.35, with NaOH. Slices (250 µm) were prepared as coronal sections on a vibratome. Before recording, slices were kept submerged in artificial cerebrospinal fluid (ACSF) containing (in mM): NaCl, 125; KCl, 2.5; NaH_2PO_4, 1.25; $NaHCO_3$, 24; $MgSO_4$, 2; $CaCl_2$, 2; glucose, 10; pH adjusted to 7.35 by bubbling with carbogen (95% O_2 and 5% CO_2).

Whole-Cell Patch Clamp Recordings

Recordings were performed at 22 ± 1 °C (or 30 ± 1 °C, Supplementary Fig. S3) in a solution containing (in mM): NaCl, 120; KCl, 2.5; NaH_2PO_4, 1.25; HEPES, 30; $MgSO_4$, 2; $CaCl_2$, 2; glucose, 10; pH 7.25. Cells were visually identified by infrared differential interference contrast video-microscopy. Currents were measured with 2–3 MΩ glass microelectrodes filled with (in mM): K-gluconate, 95; K_3-citrate, 20; NaCl, 10; HEPES, 10; $MgCl_2$, 1; $CaCl_2$, 0.5; BAPTA, 3; Mg-ATP, 3; Na_2-GTP, 0.5. Voltage-clamp experiments were controlled by the software Pulse or PatchMaster (HEKA Elektronik). The protocol was designed to increase the stability of whole-cell recordings and account for the increasingly fast activation kinetics of I_h. The pulse length was shortened by 1.5 s with every hyperpolarizing step (starting from a 17.0 s pulse length at −40 mV up to a 3.5 s pulse at −130 mV).

Steady-state activation of I_h was estimated by normalizing the mean tail current amplitudes 50–100 ms after stepping to a constant potential from a variable amplitude step using the following equation:

$$p(V) = (I - I_{min})/(I_{max} - I_{min})$$

with I_{max} being the tail current amplitude for the voltage step from −130 to −100 mV and I_{min} for the voltage step from −40 to −100 mV, respectively.

I_h activation was well accounted for by a Boltzmann equation of the following form:

$$p(V) = 1/(1 + \exp((V - V_h)/k)),$$

where V_h is the voltage of half-maximal activation and k the slope factor.

The amplitude of I_h was calculated by subtracting the instantaneous current amplitude from the steady-state current.

The time course of I_h activation in mouse TC neurons at room temperature was best approximated by the following double-exponential equation:

$$I_h(t) = A_0 + A_1 \times e^{-t/\tau 1} + A_2 \times e^{-t/\tau 2},$$

where I_h (t) is the current amplitude at time t, and A_0, A_1 and A_2, and τ_1 and τ_2 are axis intercept, amplitude coefficients, and time constants, respectively.

Under the recording conditions, no significant differences were found for the membrane capacitance of the different cell types in control and HCN4-KO: centromedial nucleus (CM), control: 70 ± 5 pF (n = 26), HCN4-KO: 73 ± 3 pF (n = 39); ventrobasal complex (VB), control: 87 ± 7 pF (n = 23), HCN4-KO: 84 ± 7 pF (n = 26); SSC, control: 71 ± 4 pF (n = 19), HCN4-KO: 79 ± 6 pF (n = 20). During experiments with 8-bromo-cyclic adenosine monophosphate (Sigma) added to the recording pipette, properties of I_h were determined 10–15 min after obtaining the whole-cell configuration.

Switch-Clamp Recording Protocol

In order to abolish potentially confounding influences of T-type Ca^{2+} channel gating on bursting of TC neurons we used a switch-clamp protocol. I_h was activated by hyperpolarizing steps (4000 ms) of −10 mV increments (−80 to −120 mV) from a holding potential of −60 mV. To compare the low-threshold spike (LTS) evoked upon different negative potentials, the amplifier was instantaneously switched to current-clamp mode (with no current injection, for 2000 ms) at the end of each hyperpolarizing step. I_h density was measured for both HCN4-KO and control VB TC neurons at each hyperpolarizing step to −120 mV. The integral areas under the rebound bursts evoked by switching from voltage-clamp to current-clamp at −80 and −120 mV were compared both between and within the 2 genotypes (HCN4-KO and control VB TC neurons).

Extracellular Recordings in Slices

Extracellular field potentials were recorded from horizontal brain slices with glass pipettes (0.5–2 MΩ) and an AC-coupled amplifier using a low pass filter of 3 kHz at 32 °C. The extracellular solution was composed of (in mM): NaCl, 124; KCl, 4; NaH_2PO_4, 1.24; $MgSO_4$, 2; $CaCl_2$, 2; $NaHCO_3$, 26; dextrose, 10; pH 7.35. Burst activity in VB was evoked by stimulation of the internal capsule through a bipolar tungsten electrode. The stimulation protocol consisted of 1, 3, 5 and 10 pulses of 1.45 mA amplitude with a duration of 1 ms each (interpulse interval 2 ms, network activity was recorded for 1 min after each stimulation). Burst firing was characterized by at least 3 high-frequency spikes with an intraburst frequency interval of >100 Hz and interburst interval of not less than 500 ms. The activity was measured 50–100 ms after the stimulation of the internal capsule for one minute. All analyzes were performed offline using Clampfit 10 (Molecular devices, USA) and Peak v1.0 (Meuth IT consulting, Germany) software.

TC Network Computer Modeling

Simulations were conducted within the NEURON simulation environment (Hines and Carnevale 2001) based on a modified version of a TC network model (Kanyshkova et al. 2009, 2012). The original model can be downloaded at http://senselab.med. yale.edu/ModelDB/ using model accession number 3343. This model comprises 2 spontaneously pacemaking TC relay neurons and 2 thalamic reticular neurons (NRT) interacting via $GABA_{A+B}$ and AMPA synapses (Supplementary Fig. S8). While NRT neuron parameters were not changed, the I_h module of both TC neurons was modified by introducing activation kinetics (τ), half-maximal activation (V_h) and conductance as measured in 14 control and 14 HCN4-KO neurons (Supplementary Table 1). The I_h amplitude of each cell was normalized to the default I_h conductance of the model (ghbar_iar = 1.0 * 10^{-5} S/cm^2). Since the original I_h module in NEURON included only single exponential activation kinetics, the slower τ_2 measured in VB TC neurons were used for the modeling approach. All parameter sets were simulated for 20 s in order to reach an equilibrium state, simulation temperature was set to 36 °C.

Single Cell Computer Modeling

Simulations were conducted within the NEURON simulation environment based on a single-compartment model of thalamic relay cells (Destexhe et al. 1998). The model can be downloaded at http://senselab.med.yale.edu/ModelDB/ using

accession number 279. This model comprises one TC neuron under current clamp mode. The I_h module was modified by introducing I_h parameters measured in 14 control and 14 HCN4-KO neurons as detailed above. All parameter sets were simulated for 2 s, simulation temperature was set to 36 °C.

Statistics

All data are expressed as mean ± standard error of the mean (S.E.M.) Student's t-tests were used for simple comparison between groups. In case of multiple comparisons, one-way ANOVA, multivariate or repeated-measures ANOVAs were used for analyses. Data were tested for normal distribution using the Kolmogorov–Smirnov test of normality. Mauchly's test of sphericity was used for repeated-measures ANOVA. Where sphericity assumption was violated ($P < 0.05$), the greenhouse-geisser correction was applied. Student's t tests were used as post hoc tests. P-values < 0.05 were considered statistically significant. Effect sizes were calculated using eta squared.

Results

Characterization of Brain-Specific HCN4 Deficient Mice

Animals carrying floxed HCN4 alleles were mated with Nestin-Cre mice (Tronche et al. 1999) (Supplementary Fig. S1A,B). In controls, strong expression of HCN4 protein was observed in thalamic samples, whereas a faint signal was seen in the cortex (Fig. 1A). As expected, no HCN4 mRNA and protein were detected in knockout brains (Fig. 1A,B, Supplementary Fig. S1C). Quantitative RT-PCR on 3 areas including 2 thalamic regions (CM, VB) and the SSC demonstrated that lack of HCN4 did not alter the mRNA expression levels of HCN1-3 isoforms (Fig. 1B). In accordance with these findings, the protein expression of HCN1 and HCN2 in thalamic and cortical samples was not different between controls and mutants (Supplementary Fig. S1D).

HCN4 is Mainly Expressed in the Thalamus

After the specificity of available anti-HCN4 antibodies had been validated using knockout brain sections, we determined HCN4 protein expression in controls. HCN4 is predominantly expressed in the thalamus (Fig. 1C,D). Highest signals were seen in the dorsal lateral geniculate nucleus (dLGN) and the ventral nuclear group of the thalamus including the ventral anterior nucleus (VA), the ventral lateral nucleus (VL) and the VB. Medium strength signals were observed in the anterior part of the paraventricular nucleus (PVA), the CM and the medial dorsal nucleus (MD) of the thalamus. In contrast, no expression was detected in the NRT. We observed low-level expression of HCN4 in the cortex and the CA1–CA3 region of the hippocampus. We also used immunofluorescence to localize the expression of HCN4 (Fig. 1D). In the somatosensory cortex, cell bodies of scattered neurons were lightly labeled. In the VB, a dense staining pattern was observed in both cell bodies and the local neuropil.

The thalamus participates in relay and processing of sensory information, control of the motor system and regulation of the sleep/wake cycle. Brain-specific HCN4-deficient mice showed no obvious abnormalities and their brain morphology as assessed by Nissl-stained sections appeared normal. We performed a battery of behavioral tests to screen HCN4-deficient animals. Tests for visual and mechanosensitive function and noxious heat perception revealed no difference between control and knockout. Similarly, motor performance and motor
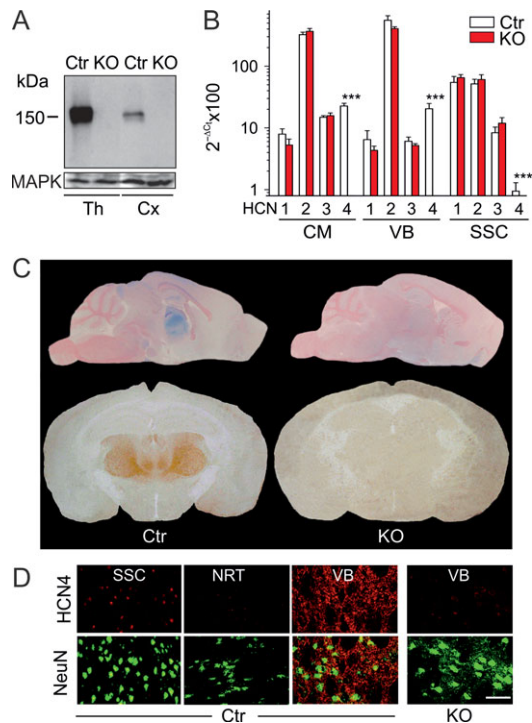
Figure 1. Characterization of brain-specific HCN4-deficient mice. (A) HCN4 protein expression in thalamus (Th) and frontal cortex (Cx) specimens from control (Ctr) and knockout (KO) mice. MAP-Kinase (MAPK), loading control. (B) Analysis of the mRNA expression of the 4 HCN isoforms in the CM, the VB and the somatosensory cortex (SSC), $n = 3/3$ KO and control mice. Isoform expression levels were not different between control and knockout except for HCN4 ($P < 0.001$). (C) Top, sagittal sections of control and knockout mice labeled with an HCN4-antibody (blue staining). Sections were counterstained with Nuclear Fast Red. Bottom, detection of HCN4 in frontal sections (DAB staining). (D) HCN4-immunofluorescence (red) in the SSC, NRT and VB. Left panels: control, right panel: HCN4-KO. Neurons were colabeled by an anti-NeuN antibody (green). Scale bar, 50 μm.

learning on an accelerating rotarod as well as circadian locomotor activity was unaltered (Supplementary Fig. S2A–E).

HCN4 is the Major Contributor to I_h in Different TC Neurons

As compared to I_h in TC neurons from control CM, VB and dLGN TC neurons, the current was strongly decreased in these areas in HCN4-deficient mice (Fig. 2A,B,D,E and Supplementary Fig. S3A,B). The mean amplitude (at −130 mV) was reduced by 84%, 58%, and 67% in knockout CM, VB, and dLGN, respectively ($P < 0.001$). In addition, significant depolarizing shifts of the activation curve in CM (V_h control: −87.2 ± 0.4 mV, $n = 15$; HCN4-KO: −82.5 ± 0.8 mV, $n = 19$; $P < 0.001$), VB (control: −86.4 ± 0.6 mV, $n = 16$; HCN4-KO: −82.9 ± 0.5 mV, $n = 14$; $P < 0.001$) and dLGN (control: −88.4 ± 0.9 mV, $n = 13$; HCN4-KO: −81.6 ± 0.9 mV, $n = 10$; $P < 0.001$) were detected (Fig. 2C,F and Supplementary Fig. S3C).

The activation time course in controls was best described by a double exponential function with fast (τ_1) and slow (τ_2) activation constants averaging 340 and 2400 ms (at −130 mV). Activation of I_h in knockout TC neurons was significantly faster with τ_1 at around 180 ms ($P < 0.001$). τ_2 was accelerated to 1230 ms in VB and dLGN, whereas CM neurons did not show a slow activation constant.

Very similar relative differences between TC neurons from control and knockout with respect to current amplitude, voltage-dependency and activation kinetics were found at a recording temperature of 30 °C (Supplementary Fig. S3E–K).

We also recorded I_h in layer 5 pyramidal neurons from the primary SSC. In contrast to the thalamus, no differences were found between control and knockout with respect to current amplitudes, activation curve and activation kinetics (Fig. 2G–I). Taken together, these findings demonstrate that HCN4 is the major contributor to I_h in a variety of TC relay neurons, whereas the isoform is not relevant in cortical pyramidal neurons.

Deletion of HCN4 Removes cAMP Modulation in CM, but not VB TC Neurons

To examine cAMP-dependent gating (Kaupp and Seifert 2001; Robinson and Siegelbaum 2003; Biel et al. 2009), we used pipette solutions containing different concentrations of 8-bromo-cAMP (1–100 μM). Cyclic AMP mediated a concentration-dependent shift of I_h activation in the positive direction in control CM TC neurons ($P < 0.001$, Fig. 3A; representative current traces are shown in Supplementary Fig. S4A). This effect was abolished in the knockout (n.s. for all cAMP concentrations as compared with control conditions without added cAMP). As a result, V_h values in the presence of 100 μM cAMP were significantly more depolarized in controls (−77.1 ± 0.8 mV, $n = 21$ cells) as compared with knockouts (−80.8 ± 1.3 mV, $n = 14$ cells, $P < 0.05$). Cyclic AMP also induced a positive shift of V_h in control VB neurons ($P < 0.001$, Fig. 3B and Supplementary Fig. S4B), however, for these neurons, the shift was preserved in the knockout. The fast kinetics and low cAMP-sensitivity of I_h in mutant CM neurons resemble the properties of cloned HCN1 channels (Santoro et al. 1998). Indeed, the HCN1-specific blocker MEL57A (Del Lungo et al. 2012) resulted in a significant reduction of the current in mutant CM neurons (30 μM, $n = 4$ cells, Fig. 3C). As expected, the HCN isoform-unselective blocker ZD7288 also blocked the current in knockout CM neurons (30 μM, $n = 4$ cells; Fig. 3C). These findings show that HCN4 is responsible for the cAMP-dependency of I_h in CM TC neurons; in contrast the subunit is not necessary for the cAMP-dependency in VB neurons.

HCN4 Increases Rebound Burst Firing and Burst Duration in TC Neurons

Tonic I_h is thought to influence membrane input resistance (R_{input}), resting membrane potential (V_{rest}) and firing properties (He et al. 2014). Indeed, R_{input} of HCN4-deficient CM TC neurons was significantly increased (366 ± 25 MΩ, $n = 29$ KO, 219 ± 13 MΩ, $n = 22$ Ctr, $P < 0.001$) and V_{rest} was significantly more hyperpolarized (−66.4 ± 0.5 mV, $n = 29$ KO; −62.0 ± 0.4 mV, $n = 22$ Ctr, $P < 0.001$, Fig. 4B) as compared with control. Similarly, V_{rest} of knockout dLGN and VB neurons was shifted by 4 and 9 mV in the hyperpolarizing direction, respectively (dLGN: −64.0 ± 0.8 mV, $n = 28$ KO vs. −59.7 ± 0.6 mV, $n = 19$ Ctr, $P < 0.001$; VB: −76.2 ± 1.3 mV $n = 7$ KO vs. −65.7 ± 1.5 mV, $n = 10$ Ctr, $P < 0.001$). VB showed a significantly more hyperpolarized V_{rest} as compared with dLGN in both knockout ($P < 0.001$) and control ($P < 0.001$) TC neurons. R_{input} of these cells was also significantly higher as compared with control (dLGN: 298.4 ± 9.9 MΩ, $n = 7$ KO vs. 201.3 ± 10.6 MΩ, $n = 7$ Ctr, $P < 0.001$; VB: 222.6 ± 20.1 MΩ, $n = 7$ KO vs. 149.6 ± 8.9, $n = 10$ Ctr; $P < 0.01$, Supplementary Fig. S5).

A hallmark of I_h activation is the depolarizing voltage sag generated during negative voltage deviations from rest. Control CM TC
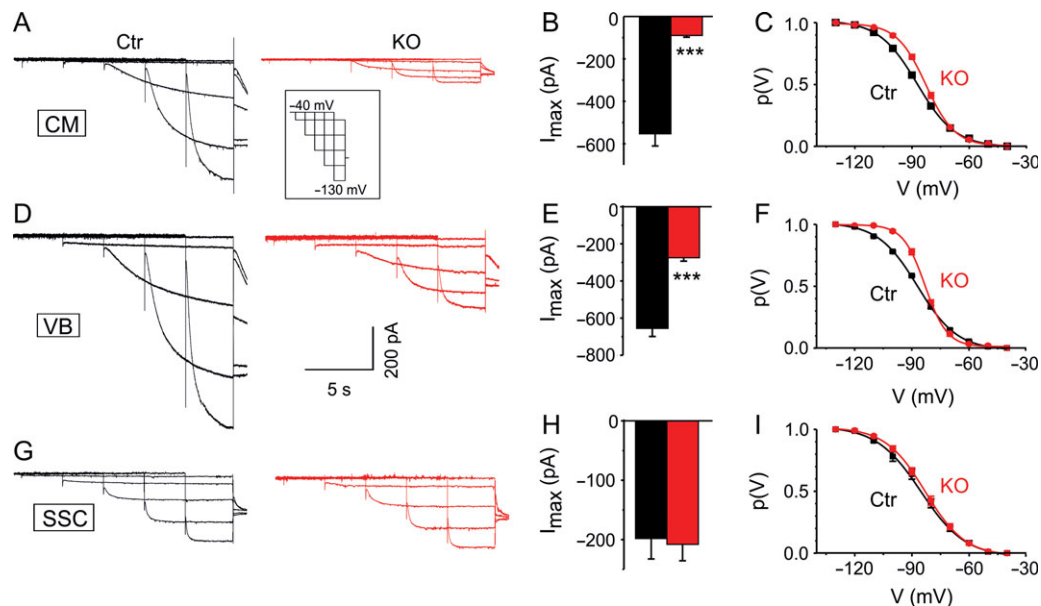
Figure 2. Contribution of HCN4 to I_h properties in thalamocortical and cortical neurons. (A) Representative I_h recordings from TC neurons in the CM nucleus from control (black) and knockout (red). (B) Mean I_h amplitudes from control and knockout CM neurons determined at −130 mV (15/19 cells, $P < 0.001$). (C) Mean I_h steady-state activation curves from CM neurons (15/19 cells). (D) Representative I_h recordings from VB TC neurons. (E) Mean current amplitudes from control and knockout VB neurons (16/14 cells, $P < 0.001$). (F) Mean steady-state activation curves from VB neurons (16/14 cells). (G) I_h recordings from layer 5 pyramidal neurons of the primary somatosensory cortex. (H) Mean current amplitudes from control and knockout SSC neurons (9/12 cells, n.s.). (I) Mean steady-state activation curves from SSC neurons (9/12 cells).
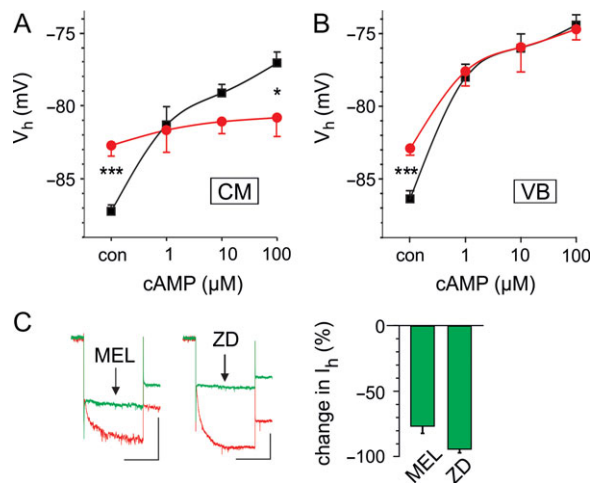

Figure 3. Cyclic-AMP-modulation of I_h and blockage of HCN channels in TC neurons. (A) V_h values at different cAMP concentrations determined from independent populations of control (black) and knockout (red) CM neurons (21/14 cells). (B) V_h values from control and knockout VB neurons (15/6 cells) at the cAMP concentrations indicated. (C) Representative current traces evoked by steps to −130 mV in knockout CM neurons in the absence (red) and presence (green) of the HCN1 blocker MEL57A (MEL, 30 μM) and ZD7288 (ZD, 30 μM). Scale bars 2 s and 50 pA. The percentage I_h reduction by MEL57A and ZD728 (each $n = 4$ cells) is shown on the right.

neurons displayed a prominent time-dependent rectification during hyperpolarization and a burst of action potentials (APs) riding on top of a LTS following release from hyperpolarization (Fig. 4A). With hyperpolarization reaching −100 mV, the voltage sag was 10.2 ± 1.6 mV ($n = 17$ cells). Deactivation of I_h generates a slow afterdepolarization contributing to LTS shape. In control CM neurons, bursts lasted 37.9 ± 5.2 ms with 3.4 ± 0.3 APs ($n = 17$ cells). In

contrast, knockouts displayed significantly reduced voltage sags (3.2 ± 0.3 mV) and shorter bursts (19.9 ± 2.6 ms) with less APs (2.1 ± 0.2, $n = 29$; $P < 0.01$, Fig. 4A–C). HCN4-deficient VB TC neurons showed similarly reduced voltage sags (2.9 ± 0.7 mV $n = 7$ KO cells vs. 12.9 ± 2.9 mV, $n = 10$ Ctr cells, $P < 0.01$, Supplementary Fig. S5A, D) and shorter bursts (19.3 ± 5.4 ms, $n = 8$, vs. 41.01 ± 8.6 ms, $n = 10$, $P < 0.05$) as compared with control cells.

In order to link the changes in bursting to loss of HCN4, I_h parameters obtained in CM TC control and knockout neurons were used in a single cell model (Fig. 4D,E). The model cell was hyperpolarized using current injection (−230 pA, 900 ms duration; black and red traces represent use of control and knockout parameters, respectively) and allowed to return to RMP thereby triggering a LTS (Fig. 4D). At the end of the hyperpolarizing pulse, 98.3% and 99.2% of T-type channels were deinactivated in control ($n = 14$) and knockout ($n = 14$) neurons. Using I_h parameters obtained from knockout TC neurons, we found a more hyperpolarized resting membrane potential together with reductions in voltage sag, AP number in a burst and burst duration (all $P < 0.001$, Fig. 4E), thereby corroborating the slice data.

We then analyzed tonic sequences of APs in CM neurons induced by injection of different depolarizing pulses from a holding potential of −55 mV (Supplementary Fig. S6A–F). The number of APs in HCN4-knockout neurons was not significantly different from control ($n = 9/8$ for Ctr and KO cells, n.s.). In addition, other AP characteristics including peak amplitude, width and afterhyperpolarization were not different between control and mutant neurons.

Injection of depolarizing pulses in VB neurons (Supplementary Fig. S5E, F) however evoked higher number of APs in HCN4-KO compared with control cells (mixed repeated-measures ANOVA showed significant interaction between the number of APs and genotype, $P = 0.011$, $n = 6/8$ for Ctr and KO; post hoc tests showed a significant difference only at +350 pA current injection, $P < 0.05$).
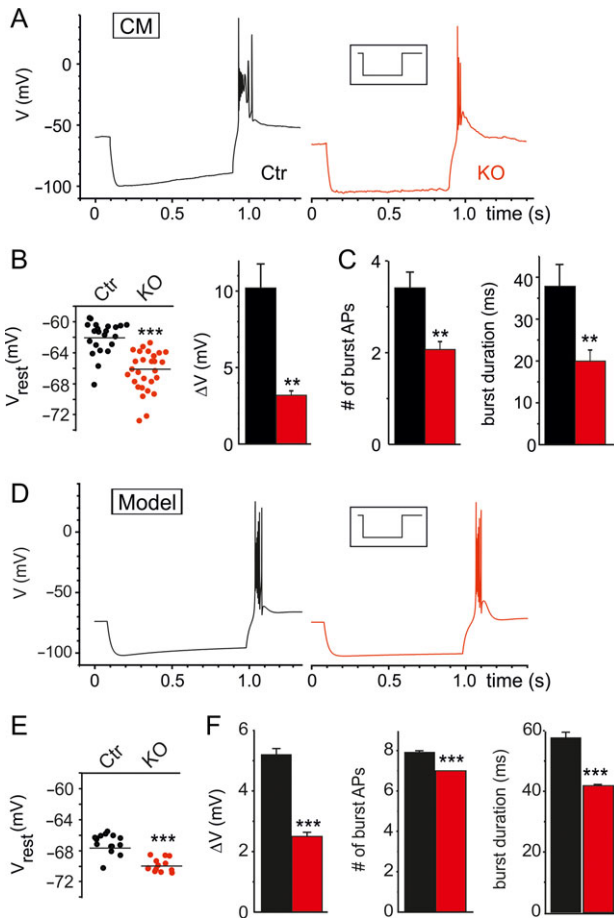
Figure 4. HCN4 determines passive membrane properties and burst firing characteristics of TC neurons. (A) Representative examples of action potential firing elicited by hyperpolarizing current pulse (800 ms duration; −200 pA, inset) from resting membrane potential in CM TC neurons from control (black trace) and knockout (red trace). (B) Resting membrane potentials of CM neurons (left) and voltage sag (right). Control ($n = 17$) and knockout ($n = 29$) neurons are indicated by black and red circles (left) and bars (right), respectively. (C) Number of APs in a burst triggered by an LTS (left) and burst duration (right). Control ($n = 17$) and knockout ($n = 29$) neurons are indicated by black and red bars, respectively. (D) Rebound burst firing of neurons in a computer model. Parameters obtained for I_h in CM TC control and knockout neurons were used for modeling. The simulation emerged from the default starting point of the single cell model (−70 mV). After 80 ms a hyperpolarizing current pulse (−230 pA, 900 ms duration) was applied, then model cells (black and red traces represent control and knockout cells respectively) returned to RMP thereby triggering a LTS. (E) Resting membrane potentials (left) and voltage sag (right) used for the modeled cells. (F) Number of APs in a burst (left) and burst duration (right) of modeled neurons. Control ($n = 14$) and knockout ($n = 14$) modeled neurons are indicated by black and red bars, respectively.

Thus, HCN4 strongly determines the bursting properties of TC neurons by facilitating anomalous rectification and prolonging burst duration.

To further investigate the bursting behavior of TC neurons upon reaching different negative voltages without the potential differential influence of T-type Ca^{2+} channel gating, a switch-clamp protocol was used (Fig. 5A). VB TC neurons of HCN4-KO mice showed a significantly lower I_h density (determined at −120 mV) as compared with control (1.7 ± 0.3 pA/pF, $n = 10$ for KO cells vs. 9.2 ± 1.2 pA/pF, $n = 8$ for Ctr cells, $P < 0.001$, Fig. 5B). Knockout neurons also showed smaller and shorter rebound bursts evoked by the switch to current-clamp from both

potentials in comparison to controls (−80 mV: 5.0 ± 1.7 mV ms vs. 134.5 ± 3.3 mV ms and −120 mV: 188.2 ± 18 mV ms vs. 304 ± 26 mV ms; =10/8 cells for KO and Ctr, $P < 0.001$, Fig. 5C).

HCN4-Deficient Animals do not Show Spontaneous Absence Epilepsy

In telemetric surface EEG recordings in freely moving animals, mutant ($n = 7$) and control ($n = 9$) animals displayed no spontaneous spike-and-wave discharge (SWD) activity (data not shown) as characterized by a rhythmic spike-and-wave pattern with spike amplitudes of at least twice the background and a spike frequency of 6–10 Hz (van Luijtelaar and Coenen 1986; Crunelli and Leresche 2002). In addition, local field potential recordings in cortex and thalamus of freely behaving knockout and control mice did not show any SWD activity (Supplementary Fig. S7). Furthermore, no other forms of pathophysiological activity (single spikes, polyspikes, or spike-complexes) were found.

HCN4 is Necessary to Sustain Intrathalamic Oscillations in Brain Slices

Rhythmic bursting of the thalamic network has frequently been used as a measure of intrathalamic rhythmicity and possible predisposition for epileptic seizures (Bal et al. 1995; Yue and Huguenard 2001; Schofield et al. 2009). To address the contribution of HCN4 to evoked thalamic oscillations, extracellular multiunit activity was recorded in VB after stimulation of corticothalamic fibers running through the internal capsule (Fig. 6A,B). The stimulation protocol consisted of series of pulses increasing in number (1–10 pulses, interpulse interval 2 ms, stimulation interval 1 min, Fig. 6C, right upper, inset). Stimulation of the internal capsule in controls resulted in a significantly higher number and longer duration of bursts for all pulse series in comparison to HCN4-KOs (for both number of bursts and duration of bursts as dependent variables: ANOVAs main effects for genotype $P < 0.05$, main effect for number/duration of pulses $P < 0.001$, interaction between genotypes and number/duration of pulses $P < 0.01$, $n = 6/6$ slices from 3 animals, Fig. 6C).

Probably based on the increasing recruitment of corticothalamic fibers and mGluR-dependent long-lasting depolarization of TC neurons, burst firing in these cells is progressively prevented (Mccormick and Vonkrosigk 1992; von Krosigk et al. 1999). Accordingly, increasing the number of pulses decreased the number and duration of bursts in both genotypes. Stimulation of the internal capsule in controls also evoked a higher number of spikes in bursts as compared with knockouts (ANOVAs $P < 0.001$, Fig. 6C).

To confirm that the strong reduction of stimulus-induced activity in knockouts resulted from the reduction of I_h, we applied ZD7288 (30 μM for 20–30 min) in control slices. Indeed, after washing-in ZD7288 stimulus-induced bursting revealed a time-dependent decrease and was eventually completely abolished ($n = 5$ slices, Fig. 6D).

To further corroborate these findings, a modeling approach was used. Spontaneous rhythmic bursting was analyzed in an intrathalamic network model able to sustain rhythmic activity (Kanyshkova et al. 2009, 2012). The model consists of 2 TC relay and 2 NRT neurons with the NRT neurons projecting to both TC neurons via GABA$_A$ and GABA$_B$ synapses (Supplementary Fig. S8). At −70 mV and I_h properties from control VB neurons, both TC neurons generated spontaneous burst activity with a frequency of around 3 Hz (Fig. 6E,F). I_h properties in TC neurons were then set to mimic the individual combinations of current
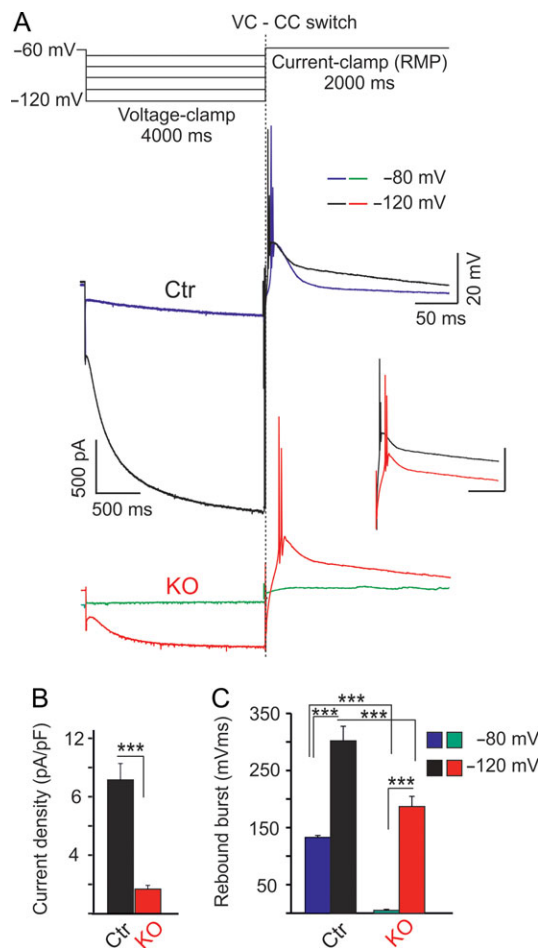
Figure 5. Changes in firing pattern of VB TC neurons by lack of HCN4. (A) A switch-clamp protocol was used for analyzing bursting in order to abolish potential confounding influences of T-type Ca^{2+} channel gating. Top: Switch-clamp protocol. I_h was activated by hyperpolarizing steps (4000 ms) of −10 mV increments from a holding potential of −60 mV. To compare the LTS evoked upon different negative potentials, the amplifier was instantaneously switched to current-clamp mode (with no current injection) at the end of each hyperpolarizing step. Representative I_h (left, voltage-clamp) and LTS (right, current-clamp) recordings from VB TC neurons from control (blue and black traces) and HCN4-KO (green and red traces) are shown. The inset shows bursts evoked by switching from −120 mV. Bars indicate 50 ms and 20 mV, respectively. (B) I_h density in control and knockout VB TC neurons measured at the step to −120 mV. (C) Integral area under the rebound burst evoked by switching from voltage-clamp (at −80 and −120 mV) to current clamp (8/10 cells, $P < 0.001$). Knockout neurons showed smaller and shorter rebound bursts evoked by the switch to current-clamp in comparison to controls.

amplitude, V_h, k, and activation kinetics observed in knockout cells (Supplementary Table S1). NRT neuron properties were left unaltered since HCN4 was not detected in these cells. Compared with control, the frequency of the network oscillation was significantly slower (2.9 ± 0.1 Hz, $n = 14$ controls; 2.2 ± 0.1 Hz, $n = 14$ knockouts, $P < 0.001$) and the number of bursts was significantly reduced (Fig. 6E,F). Furthermore, in 15% of the trials using knockout parameters no rhythmic network activity was generated, whereas all runs with control parameters resulted in rhythmic activity. Taken together, rhythmic thalamic bursting in a computational model was slowed down by removal of HCN4 indicating that a critical amount of I_h is necessary to sustain intrathalamic oscillations. In the horizontal slice preparation, the decrease of I_h density by either HCN4 deletion

or pharmacological block is sufficient to reduce and eventually prevent stimulus-induced bursting.

To assess cortical function, TC slices with preserved connections between the thalamus and cortex were investigated (Supplementary Fig. S9A). Following electrical stimulation in VB, no significant differences in the amplitude of evoked population spikes between HCN4-KO and control were observed ($P = 0.19$, effect size = 0.16, $n = 6/6$ slices from 3 animals, Supplementary Fig. S9B). These data indicate that basic synaptic function in the cortex is not affected by loss of HCN4.

Reduction of Thalamic I_h Slows Down Thalamic and Cortical Oscillations in Vivo

The interplay between conductances including I_h and I_T, is a key factor in the generation of slow TC oscillations, especially delta and spindle oscillations (Kanyshkova et al. 2009). We obtained electrical brain activity from the SSC and the ventral–posterior medial nucleus of the thalamus (VPM) by local field potential recordings in freely moving animals (Fig. 7A–C). The peak power spectral densities (PSD) for 4 different frequency bands (delta, 1–4 Hz; theta, 4.5–8 Hz; alpha, 8.5–11 Hz; β, 11.5–30 Hz) were analyzed during epochs of active-wakefulness and slow-wave sleep. HCN4-knockouts displayed significantly slower cortical (Fig. 7B) and thalamic (Fig. 7C) oscillations during episodes of active wakefulness with a prominent increase in delta frequency band for both SSC ($P < 0.001$, $n = 3/7$) and VPM ($P < 0.01$) and a consequent decrease in higher frequencies. The percentage of peak PSD between the 2 genotypes during episodes of active-wakefulness also revealed a significant increase in delta frequency oscillations (SSC $P < 0.01$; VPM $P < 0.05$). In contrast, oscillatory activity during slow-wave sleep was similar between mutants and controls (Repeated measures ANOVA; eta-squared = 0.005 and 0.12 for genotypes and for interaction between genotypes and different frequency bands, respectively). Our results show that thalamic I_h is one of the main determinants of normal TC oscillatory activity and indicate that the reduction of I_h in relay neurons is responsible for the slowing of these oscillations.

Discussion

The present work studies the function of the HCN4 channels by examining a brain-specific deletion of the isoform. We used the knockout as stringent control for immunohistochemical analyses, which showed that HCN4 is predominantly expressed in the thalamus. In line with this expression pattern, loss of HCN4 resulted in a massive reduction of I_h in various TC neurons. HCN4 represents a prominent constituent of I_h in sensory TC neurons; its deletion resulted in a reduction of about 60% of current amplitude in dLGN and VB TC neurons. In intralaminar TC neurons, the contribution of HCN4 to I_h is even larger (about 85%). The residual I_h in mutant neurons was generally activated faster and at more depolarized potentials compared with controls. Based on the biophysical properties of cloned HCN isoforms (Wahl-Schott and Biel 2009), the remaining current in VB TC neurons seems to be carried by HCN2. The preserved effect of cyclic AMP in knockout VB neurons is probably due to the cyclic AMP-sensitive HCN2 channels that are sufficient to saturate V_h. In intralaminar TC neurons, the small residual I_h in mutants showed a highly diminished cAMP-sensitivity and was strongly reduced by an HCN1 blocker indicating that it is mainly carried by HCN1.

Tonic activation of HCN channels has been proposed to stabilize the resting membrane potential of neurons (He et al. 2014). In addition, the deactivation of the channels following
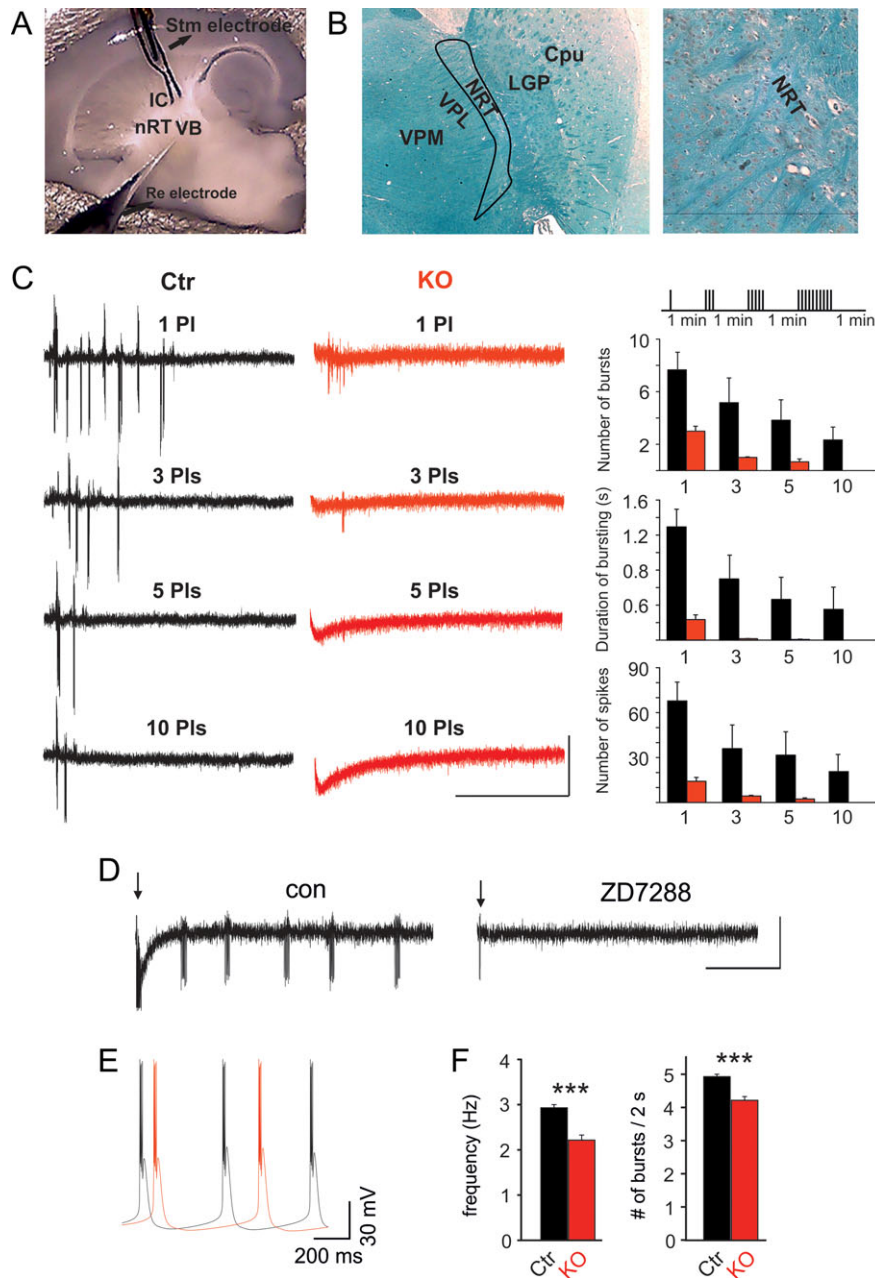
Figure 6. Thalamic burst activity in slices is strongly dependent on HCN4. (A) Position of recording (Re) and stimulation (Stm) electrodes for extracellular field potential (EFP) recordings in horizontal thalamic slices. (B) Luxol Fast Blue myelin staining on paraffin sections in HCN4 knockout horizontal slices indicating that the connections between NRT and VPM are preserved in these animals. (C) EFP recordings showing repetitive burst activity evoked by different numbers of stimulation pulses (Pls). Burst activity in VB was evoked by stimulation of the internal capsule (IC) with the protocol shown at the top right. One, 3, 5, and 10 pulses (1.45 mA, 1 ms, interpose interval of 2 ms, interval between stimulations 1 min) were applied. Calibration bars represent 2 s and 0.1 mV, respectively. On the right, the mean number of evoked bursts (top), the mean burst duration (middle) and the total number of spikes (bottom) are shown. HCN4-KO slices showed significantly lower burst number, burst duration and total spike number as compared with controls at all stimulation intensities (mixed repeated-measures ANOVA followed by Student's t-tests, main effect for number of pulses $P < 0.001$; main effect for genotype $P < 0.05$, $n = 6/6$; interaction for number of pulses and genotypes; $P < 0.01$). (D) Rhythmic burst activity under control conditions (con) and after application of 30 μM ZD7288 for 30 min. Arrows indicate the stimulus artifact; scale bars, 500 ms and 50 μV. (E) Modeling data. Results in both TC neurons of the model were identical; hence membrane potential oscillations of one TC neuron are shown for control and HCN4-KO. (F) Interburst frequency (in the first second of the modeling period) and burst number (in the first 2 s) for control and HCN4-KO.

release from hyperpolarization has been suggested to generate an afterdepolarization contributing to burst firing activity (Pape 1996; Wahl-Schott and Biel 2009). Our results provide direct evidence for these suggestions. Lack of HCN4 resulted in a hyperpolarized resting membrane potential and an increase in input resistance.

Several mechanisms may contribute to the varying degree of membrane potential changes in different thalamic nuclei. The resting membrane potentials of TC neurons from various species and thalamic nuclei are in the range of about −55 to −75 mV, and a value of −58 mV has been reported for mouse dLGN (Meuth et al. 2006; Liu et al. 2015). In thalamic neurons,
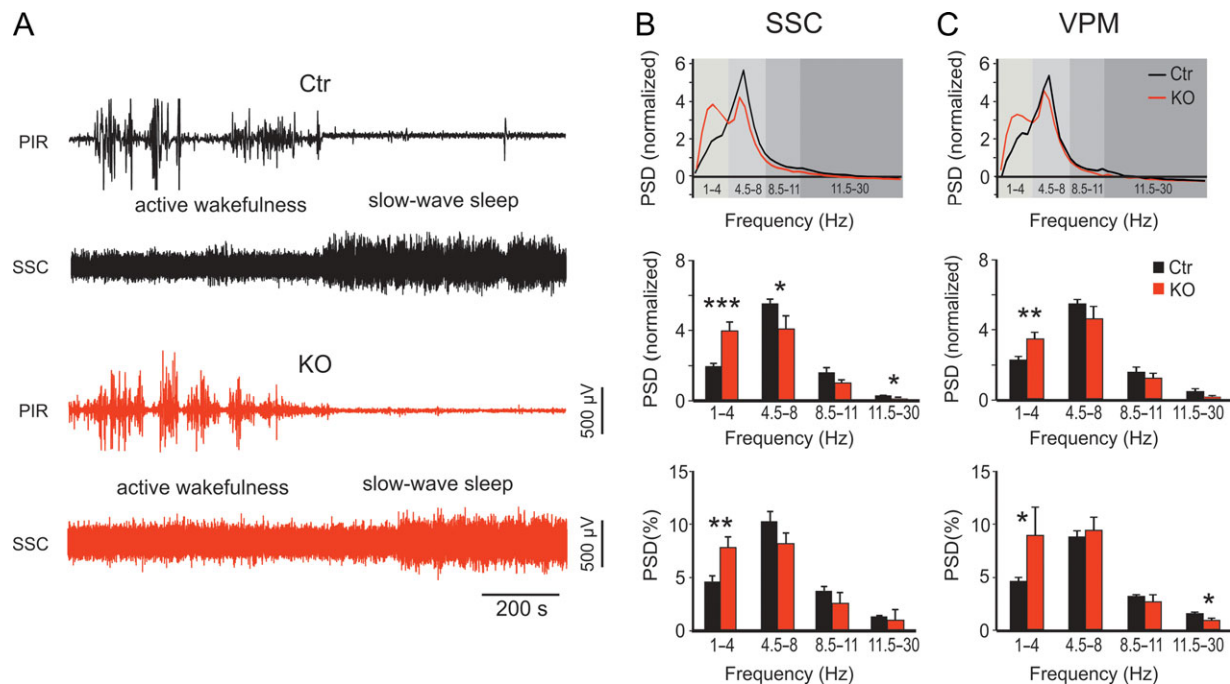
Figure 7. Slower cortical and thalamic network oscillations in HCN4-KO mice. (A) Representative local field potential recordings from the SSC of control (black, top) and HCN4-knockout (red, bottom) during active wakefulness and slow-wave sleep. The signal from the infrared movement detector (PIR) is shown in the upper traces. High-amplitude PIR signals indicate bodily activity. (B) Top: Representative spectrograms indicating the mean power spectral density (normalized, z-score) of 4 different frequency bands in the SSC during active-wakefulness in HCN4-KO (red) and control (black). Middle: Comparison of the normalized peak frequency PSD (z-score) of 4 frequency bands in the SSC during active-wakefulness. Note the significant increase in delta frequency oscillations (1–4 Hz) in HCN4-KOs and a consequent decrease in higher frequencies. N = 3/7 animals for knockout and control, respectively. Bottom, Percentage of peak PSD. (C) Top, Spectrograms indicating the normalized PSD (z-score) in the ventral–posterior medial nucleus of the thalamus (VPM) during episodes of active-wakefulness. Middle, Normalized peak frequency in the VPM. Bottom, Percentage of the peak PSD during active-wakefulness indicating the significant increase in delta (1–4 Hz) and decrease in β (11.5–30 Hz) frequency bands in knockout VPM as compared with control.

the functional interaction between HCN, 2 pore domain K^+ (K_{2P}) and inward rectifier K^+ channels as well as the influence of GABAergic local circuit interneurons (IN) and NRT neurons set the magnitude of the resting membrane potential (Bista et al. 2015). While the expression levels of different K_{2P} channel subtypes in rodent sensory relay nuclei seem to be roughly similar (Karschin et al. 2001; Talley et al. 2001), the number of GABAergic IN in dLGN exceeds their number in VB (Sherman and Guillery 2006). Since IN in mouse dLGN express functional HCN4 channels and show spontaneous AP firing at depolarized membrane potentials in brain slices (Leist et al. 2016, 2017), the loss of HCN4 may hyperpolarize IN thereby disinhibiting and depolarizing dLGN TC neurons. In VB TC neurons, the hyperpolarizing shift seems to be dominated by the massive loss of I_h which has a remarkable high amplitude in control mice. In addition, rebound burst firing was strongly reduced when HCN4-deficient TC neurons were challenged with hyperpolarizing current steps. The observed shortening of the burst duration in HCN4-lacking TC neurons can be explained by the slow deactivation of HCN4 being open during the burst and thereby contributing to lengthening the burst. Furthermore, the hyperpolarizing shift of the resting membrane potential of TC neurons observed in the HCN2-knockout (−12 mV) is larger than in the HCN4 mutant (−4 mV). This difference could also be due to several reasons. It may be related to the different genetic background of the 2 lines (mixed Sv129/C57BL/6 vs. C57BL/6). In addition, the residual I_h around the resting membrane potential in the dLGN is larger in the HCN4-KO than in the HCN2-KO (−15.3 ± 2.2 pA, n = 10 cells vs. −4.1 ± 0.6 pA, n = 17 cells, at

−70 mV) exerting a stronger depolarizing effect. Another possible explanation stems from the fact that TC neurons are tonically inhibited by GABAergic neurons of the NRT and IN (Sherman and Guillery 2006; Bright et al. 2007). Specific block of HCN4 channels by EC18 resulted in membrane hyperpolarization and reduction of AP firing in IN (Leist et al. 2016; Romanelli et al. 2019). Since there are indications that HCN4 is more abundant in IN than HCN2 (Leist et al. 2016), knockout of HCN4 may result in a more pronounced loss of tonic inhibition of TC neurons as compared with loss of HCN2. As a result, the resting membrane potential of TC neurons in the HCN4-KO may be more depolarized as compared with the HCN2-KO line.

We found that neurons of both SSC and NRT, 2 regions important for the initiation, maintenance and termination of SWD activity (Luttjohann et al. 2014), do not express HCN4. Intrinsic bursting relies on persistent Na^+ channels in cortical pyramidal cells and T-type Ca^{2+} channels in NRT neurons (Franceschetti et al. 1995; Cueni et al. 2008; Ehling et al. 2013; Kanyshkova et al. 2014). Our study extends these findings by demonstrating that TC neurons possess a unique mechanism for pacemaking and bursting, which is dependent on HCN4 channels. In the thalamic network with intact connections between VB and NRT, where additional factors influence rhythmic bursting, the reduction of I_h was sufficient to strongly reduce intrathalamic oscillations. Hence, our results directly demonstrate that a critical amount of I_h in TC neurons is necessary to sustain rhythmic intrathalamic oscillations (Yue and Huguenard 2001).

Several animal models were used to determine concepts of SWD generation in rodents (Pinault and O'Brien 2005; van

Luijtelaar and Sitnikova 2006; Leresche et al. 2012). In WAG/Rij rats, SWDs seem to start from the facial area of SSC, quickly spreading over the cortex and invade the thalamus, which provides a resonance circuitry for the amplification, spreading and entrainment. Consequently somatosensory thalamic nuclei like VB and the posterior nucleus reveal strong involvement (Luttjohann et al. 2014). While these findings seem to indicate that VB is more crucial for the occurrence of SWDs than the dLGN, the latter has been shown to also sustain this type of epileptic activity (Guyon et al. 1993). HCN2 deficiency was associated with SWD generation (Ludwig et al. 2003; Chung et al. 2009), whereas in HCN4-KO mice no spontaneous SWD activity was found. Considering that SWDs need an intact TC system (both cortex and thalamus are involved), the different expression pattern of the 2 isoforms in cortex and thalamus might explain the absence of SWDs in HCN4 compared with HCN2 knockout mice. While HCN2 is strongly expressed in both cortex and thalamus, HCN4 expression is highly restricted to the thalamus. We showed that loss of HCN4 affected I_h only in thalamic nuclei, whereas the current was completely intact in cortical pyramidal neurons. In genetic absence models, for example, in WAG/Rij rats, the SSC serves as epileptic focus and primary pacemaker for SWD generation (van Luijtelaar and Zobeiri 2014). A strong reduction of I_h in cortical pyramidal neurons may explain why this region is hyperexcitable in WAG/Rij rats and the initiation site of SWDs (Strauss et al. 2004; Sitnikova and van Luijtelaar 2006). In addition, the reduction of I_h in HCN4 mutants resulted in a more hyperpolarized V_{rest}, particularly in VB TC neurons, which might in turn favor low frequency delta oscillations rather than SWDs. The above discussion is further complicated by findings obtained from mice lacking the auxiliary HCN subunit TRIP8b. While TRIP8b deficient mice (TRIP8b$^{-/-}$) revealed strongly decreased I_h in thalamus and cortex, additional compensatory mechanisms (e.g., reduced basal cAMP levels altered function of the transient K^+ current, I_A) resulted in a phenotype with sparse if any clear SWD activity and a prominent increase in the delta frequency band during episodes of active wakefulness (Heuermann et al. 2016; Zobeiri, Chaudhary et al. 2018).These findings indicate that subtle adjustments of intrinsic and network mechanisms determine the phenotype of oscillatory activity in the TC system. The recent finding that pharmacological block and knockdown of HCN channels in VB abolished SWD activity in GAERS rats and reduced absence seizures in Stargazer mice, respectively, highlights the significant role of HCN channels in VB for epileptic seizures in the TC system (David et al. 2018).

In addition to the regional differences in the expression of the 2 isoforms, the compartmental distribution also varies. HCN2 was found to be localized to dendritic spines in VB TC neurons, whereas HCN4 was primarily somatic (Abbas et al. 2006). This difference in the subcellular expression of HCN2 and HCN4 may also contribute to the different phenotype of the corresponding knockout lines with HCN2 being positioned to constrain excitatory synaptic input (Ying et al. 2007). Furthermore, newly identified HCN channel regulators may influence TC activity (Silbernagel et al. 2018).

The expression of HCN channels is also strongly age-dependent. In cortical pyramidal neurons of Wistar rats an increase in HCN1 protein levels in the first 3 months of life has been reported, while in WAG/Rij rats, a genetic model of absence epilepsy, a decrease of cortical HCN1 precedes the onset of SWDs (Kole et al. 2007). In TC neurons, there is a steady increase of HCN4 (as well as HCN1 and HCN2) during postnatal development (Kanyshkova et al. 2009, 2012). These

changes in the expression profile are accompanied by the maturation of sleep-related slow oscillations (Kanyshkova et al. 2012). In contrast, HCN4 is strongly expressed perinatally in the rodent cortex, but is dramatically decreased in the more mature cortex (Battefeld et al. 2012). The divergent developmental profile of HCN4 in TC neurons (age-dependent increase) versus cortical cells (massive reduction) underscores the region-specific function of the channel. Moreover, the strong decrease of HCN4 in cortical neurons suggests that the channel might become progressively less important in these cells up to the adult stage, where we found cortical neurons to be normal in the absence of HCN4.

HCN4-KO mice revealed a significant increase in low-frequency oscillations in thalamus and cortex during active wakefulness, which represents the manifestation of a TC dysrhythmia (TCD) (Llinas et al. 1999; Zhang et al. 2009; Schulman et al. 2011). TCD, an increase in delta or theta oscillations during wakefulness characterizes a number of neurological and neuropsychiatric disorders (Sarnthein et al. 2005; Sarnthein and Jeanmonod 2008; Zhang et al. 2009). TCD might spread in 2 different ways: a bottom-up mechanism in which dysrhythmia is triggered from thalamus towards cortex and a top-down mechanism where dysrhythmia propagates from cortex towards thalamus (Llinas et al. 1999). In both cases, a membrane hyperpolarization of TC neurons results in the generation of pathological slow oscillations. The HCN4-KO represents the bottom-up mechanism since the hyperpolarization of TC cells following loss of HCN4 resulted in low-frequent cortical oscillations. Furthermore, it is interesting to note that the SWD frequency (7–11 Hz) in genetic epilepsy models and the lower delta frequency oscillations (1–4 Hz) in TDC models are associated with increased (Kanyshkova et al. 2012) and decreased (Datunashvili et al. 2018; Zobeiri, Chaudhary et al. 2018) availability of I_h in TC neurons. Thalamic oscillatory activity is shaped by phasic inhibition of TC neurons via GABAergic NRT neurons and IN (von Krosigk et al. 1993; Lorincz et al. 2009). While HCN4 was not detected in the NRT, the channels are functionally expressed in IN (Leist et al. 2016). Therefore, the possibility exists that loss of HCN4 may influence oscillatory activity also due to an altered IN function. Interestingly, the HCN3 isoform which has low mRNA abundance in most of the brain (Moosmang et al. 1999), reveals strong protein expression in certain cell types including dLGN IN (Notomi and Shigemoto 2004). However, the role of this isoform in TCD is unclear. Cells of the intergeniculate leaflet of the thalamus, which is part of the main pathway of the circadian system, also reveal strong HCN3 expression (Stieglitz et al. 2018). While a highly significant association between EEG evidence of severe bilateral TCD and chronic sleep/wake dysregulation has been found in children (Jan et al. 2011), the knockout of HCN3 in mice did not result in changed circadian functions (Stieglitz et al. 2018).

An increase in slow-frequency delta range TC oscillations due to reduction in I_h availability has been demonstrated in several studies (Datunashvili et al. 2018; Zobeiri, Chaudhary et al. 2018) Nevertheless, there is a complex dependency of the frequency of TC oscillations on the availability of I_h and the level of hyperpolarization of thalamic neurons. While a slightly decreased I_h availability was associated with an increased frequency of intrathalamic bursting, strong reduction of I_h slowed down the frequency of oscillations to the delta range (Kanyshkova et al. 2009). Only very low levels of available I_h were associated with the loss of slow activity (Yue and Huguenard 2001). It has been proposed that additional factors like the degree of hyperpolarization of thalamic neurons which may allow bursting from RMP, alterations of other ion channels involved in burst generation, regionally restricted changes in I_h

properties, reduction in basal cAMP levels, the presence of variant HCN channels and alterations in TC connectivity may determine the occurrence of increased slow delta activity vs. SWD generation (Ludwig et al. 2003; Kanyshkova et al. 2012; Wemhöner et al. 2015; Zobeiri, Chaudhary et al. 2018; Zobeiri, van Luijtelaar et al. 2018).

In general, the phenotype of the brain-specific HCN4 knockout animals appears to be rather mild. It is possible that more subtle defects including, for example, attentional or emotional deficits may be present. We would like to note that we observed a difference in open field behavior (total distance traveled and number of rears was significantly lower in mutants, data not shown) which was not further examined here. We will investigate this finding in future studies. In this respect it interesting to note that the selective knock-down of HCN4 channels in the dorsal hippocampus of mice had an anxiogenic effect (Günther et al. 2019).

Taken together, lack of HCN4 resulted in a decreased burst activity of TC neurons, a strongly reduced bursting in the intrathalamic network and a slowing of thalamic and cortical oscillations during wakefulness. We propose that HCN4 is important for the production of rhythmic intrathalamic oscillations and determines the regular TC oscillatory activity during alert states.

Supplementary Material

Supplementary material is available at *Cerebral Cortex* online.

Funding

Notes

References

Abbas SY, Ying SW, Goldstein PA. 2006. Compartmental distribution of hyperpolarization-activated cyclic-nucleotide-gated channel 2 and hyerpolarization-activated cyclic-nucleotide-gated channel 4 in thalamic reticular and thalamocortical relay neurons. Neuroscience. 141:1811–1825.

Bal T, von Krosigk M, McCormick DA. 1995. Role of the ferret perigeniculate nucleus in the generation of synchronized oscillations in vitro. J Physiol. 483:665–685.

Battefeld A, Rocha N, Stadler K, Brauer AU, Strauss U. 2012. Distinct perinatal features of the hyperpolarization-activated non-selective cation current I(h) in the rat cortical plate. Neural Dev. 7:21.

Biel M, Wahl-Schott C, Michalakis S, Zong X. 2009. Hyperpolarization-activated cation channels: from genes to function. Physiol Rev. 89:847–885.

Bista P, Cerina M, Ehling P, Leist M, Pape HC, Meuth SG, Budde T. 2015. The role of two-pore-domain background K(+) (K(2)p) channels in the thalamus. Pflugers Arch. 467:895–905.

Blumenfeld H, Klein JP, Schridde U, Vestal M, Rice T, Khera DS, Bashyal C, Giblin K, Paul-Laughinghouse C, Wang F, et al. 2008. Early treatment suppresses the development of spike-wave epilepsy in a rat model. Epilepsia. 49:400–409.

Bright DP, Aller MI, Brickley SG. 2007. Synaptic release generates a tonic GABA(A) receptor-mediated conductance that modulates burst precision in thalamic relay neurons. J Neurosci. 27:2560–2569.

Chung WK, Shin M, Jaramillo TC, Leibel RL, LeDuc CA, Fischer SG, Tzilianos E, Gheith AA, Lewis AS, Chetkovich DM. 2009. Absence epilepsy in apathetic, a spontaneous mutant mouse lacking the h channel subunit, HCN2. Neurobiol Dis. 33:499–508.

Crunelli V, Leresche N. 2002. Childhood absence epilepsy: genes, channels, neurons and networks. Nat Rev Neurosci. 3:371–382.

Cueni L, Canepari M, Lujan R, Emmenegger Y, Watanabe M, Bond CT, Franken P, Adelman JP, Luthi A. 2008. T-type Ca2+ channels, SK2 channels and SERCAs gate sleep-related oscillations in thalamic dendrites. Nat Neurosci. 11:683–692.

Datunashvili M, Chaudhary R, Zobeiri M, Lüttjohann A, Mergia E, Baumann A, Balfanz S, Budde B, van Luijtelaar G, Pape HC, et al. 2018. Modulation of hyperpolarization-activated inward current and thalamic activity modes by different cyclic nucleotides. Front Cell Neurosci. 12:369.

David F, Carcak N, Furdan S, Onat F, Gould T, Meszaros A, Di Giovanni G, Hernandez VM, Chan CS, Lorincz ML, et al. 2018. Suppression of hyperpolarization-activated cyclic nucleotide-gated channel function in thalamocortical neurons prevents genetically determined and pharmacologically induced absence seizures. J Neurosci. 38:6615–6627.

Del Lungo M, Melchiorre M, Guandalini L, Sartiani L, Mugelli A, Koncz I, Szel T, Varro A, Romanelli MN, Cerbai E. 2012. Novel blockers of hyperpolarization-activated current with iso-form selectivity in recombinant cells and native tissue. Br J Pharmacol. 166:602–616.

Destexhe A, Neubig M, Ulrich D, Huguenard J. 1998. Dendritic low-threshold calcium currents in thalamic relay cells. J Neurosci. 18:3574–3588.

Ehling P, Cerina M, Meuth P, Kanyshkova T, Bista P, Coulon P, Meuth SG, Pape HC, Budde T. 2013. Ca(2+)-dependent large conductance K(+) currents in thalamocortical relay neurons of different rat strains. Pflügers Arch. 465:469–480.

Franceschetti S, Guatteo E, Panzica F, Sancini G, Wanke E, Avanzini G. 1995. Ionic mechanisms underlying burst firing in pyramidal neurons: intracellular study in rat sensorimotor cortex. Brain Res. 696:127–139.

Günther A, Luczak V, Gruteser N, Abel T, Baumann A. 2019. HCN4 knockdown in dorsal hippocampus promotes anxiety-like behavior in mice. Genes Brain Behav. 18(2):e12550.

Guyon A, Vergnes M, Leresche N. 1993. Thalamic low threshold calcium current in a genetic model of absence epilepsy. Neuroreport. 4:1231–1234.

He C, Chen F, Li B, Hu Z. 2014. Neurophysiology of HCN channels: from cellular functions to multiple regulations. Prog Neurobiol. 112:1–23.

Heuermann RJ, Jaramillo TC, Ying SW, Suter BA, Lyman KA, Han Y, Lewis AS, Hampton TG, Shepherd GMG, Goldstein PA, et al. 2016. Reduction of thalamic and cortical I-h by deletion of TRIP8b produces a mouse model of human absence epilepsy. Neurobiol Dis. 85:81–92.

Hines ML, Carnevale NT. 2001. NEURON: a tool for neuroscientists. Neuroscientist. 7:123–135.

Huang Z, Walker MC, Shah MM. 2009. Loss of dendritic HCN1 subunits enhances cortical excitability and epileptogenesis. J Neurosci. 29:10979–10988.

Huber R, Deboer T, Tobler I. 2000. Effects of sleep deprivation on sleep and sleep EEG in three mouse strains: empirical data and simulations. Brain Res. 857:8–19.

Jan JE, Ribary U, Wong PK, Reiter RJ, Bax MC, Wasdell MB. 2011. Cerebral modulation of circadian sleep-wake rhythms. J Clin Neurophysiol. 28:165–169.

Kanyshkova T, Ehling P, Cerina M, Meuth P, Zobeiri M, Meuth SG, Pape HC, Budde T. 2014. Regionally specific expression of high-voltage-activated calcium channels in thalamic nuclei of epileptic and non-epileptic rats. Mol Cell Neurosci. 61:110–122.

Kanyshkova T, Meuth P, Bista P, Liu Z, Ehling P, Caputi L, Doengi M, Chetkovich DM, Pape HC, Budde T. 2012. Differential regulation of HCN channel isoform expression in thalamic neurons of epileptic and non-epileptic rat strains. Neurobiol Dis. 45:450–461.

Kanyshkova T, Pawlowski M, Meuth P, Dube C, Bender RA, Brewster AL, Baumann A, Baram TZ, Pape HC, Budde T. 2009. Postnatal expression pattern of HCN channel isoforms in thalamic neurons: relationship to maturation of thalamocortical oscillations. J Neurosci. 29:8847–8857.

Karschin C, Wischmeyer E, Preisig-Müller R, Rajan S, Derst C, Grzeschik KH, Daut J, Karschin A. 2001. Expression pattern in brain of TASK-1, TASK-3, and a tandem pore domain K(+) channel subunit, TASK-5, associated with the central auditory nervous system. Mol Cell Neurosci. 18:632–648.

Kaupp UB, Seifert R. 2001. Molecular diversity of pacemaker ion channels. Annu Rev Physiol. 63:235–257.

Kole MH, Brauer AU, Stuart GJ. 2007. Inherited cortical HCN1 channel loss amplifies dendritic calcium electrogenesis and burst firing in a rat absence epilepsy model. J Physiol. 578: 507–525.

Leist M, Datunashvili M, Kanyshkova T, Zobeiri M, Aissaoui A, Cerina M, Romanelli MN, Pape HC, Budde T. 2016. Two types of interneurons in the mouse lateral geniculate nucleus are characterized by different h-current density. Sci Rep. 6: 24904.

Leist M, Rinne S, Datunashvili M, Aissaoui A, Pape HC, Decher N, Meuth SG, Budde T. 2017. Acetylcholine-dependent upregulation of TASK-1 channels in thalamic interneurons by a smooth muscle-like signalling pathway. J Physiol. 595: 5875–5893.

Leresche N, Lambert RC, Errington AC, Crunelli V. 2012. From sleep spindles of natural sleep to spike and wave discharges of typical absence seizures: is the hypothesis still valid? Pflügers Arch. 463:201–212.

Liu T, Petrof I, Sherman SM. 2015. Modulatory effects of activation of metabotropic glutamate receptors on GABAergic circuits in the mouse thalamus. J Neurophysiol. 113:2646–2652.

Llinas RR, Ribary U, Jeanmonod D, Kronberg E, Mitra PP. 1999. Thalamocortical dysrhythmia: a neurological and neuropsychiatric syndrome characterized by magnetoencephalography. Proc Natl Acad Sci USA. 96:15222–15227.

Lorincz ML, Kekesi KA, Juhasz G, Crunelli V, Hughes SW. 2009. Temporal framing of thalamic relay-mode firing by phasic inhibition during the alpha rhythm. Neuron. 63:683–696.

Ludwig A, Budde T, Stieber J, Moosmang S, Wahl C, Holthoff K, Langebartels A, Wotjak C, Munsch T, Zong X, et al. 2003. Absence epilepsy and sinus dysrhythmia in mice lacking the pacemaker channel HCN2. EMBO J. 22:216–224.

Ludwig A, Flockerzi V, Hofmann F. 1997. Regional expression and cellular localization of the alpha1 and beta subunit of high voltage-activated calcium channels in rat brain. J Neurosci. 17:1339–1349.

Ludwig A, Zong X, Jeglitsch M, Hofmann F, Biel M. 1998. A family of hyperpolarization-activated mammalian cation channels. Nature. 393:587–591.

Lüttjohann A, Schoffelen JM, van Luijtelaar G. 2014. Termination of ongoing spike-wave discharges investigated by cortico-thalamic network analyses. Neurobiol Dis. 70: 127–137.

Mccormick DA, Vonkrosigk M. 1992. Corticothalamic activation modulates thalamic firing through glutamate metabotropic receptors. Proc Natl Acad Sci USA. 89:2774–2778.

Meuth SG, Kanyshkova T, Meuth P, Landgraf P, Munsch T, Ludwig A, Hofmann F, Pape HC, Budde T. 2006. Membrane resting potential of thalamocortical relay neurons is shaped by the interaction among TASK3 and HCN2 channels. J Neurophysiol. 96:1517–1529.

Monteggia LM, Eisch AJ, Tang MD, Kaczmarek LK, Nestler EJ. 2000. Cloning and localization of the hyperpolarization-activated cyclic nucleotide-gated channel family in rat brain. Brain Res Mol Brain Res. 81:129–139.

Moosmang S, Biel M, Hofmann F, Ludwig A. 1999. Differential distribution of four hyperpolarization-activated cation channels in mouse brain. Biol Chem. 380:975–980.

Nolan MF, Malleret G, Dudman JT, Buhl DL, Santoro B, Gibbs E, Vronskaya S, Buzsaki G, Siegelbaum SA, Kandel ER, et al. 2004. A behavioral role for dendritic integration: HCN1 channels constrain spatial memory and plasticity at inputs to distal dendrites of CA1 pyramidal neurons. Cell. 119: 719–732.

Nolan MF, Malleret G, Lee KH, Gibbs E, Dudman JT, Santoro B, Yin D, Thompson RF, Siegelbaum SA, Kandel ER, et al. 2003. The hyperpolarization-activated HCN1 channel is important for motor learning and neuronal integration by cerebellar purkinje cells. Cell. 115:551–564.

Notomi T, Shigemoto R. 2004. Immunohistochemical localization of Ih channel subunits, HCN1-4, in the rat brain. J Comp Neurol. 471:241–276.

Pape H-C. 1996. Queer current and pacemaker: the hyperpolarization-activated cation current in neurons. Annu Rev Physiol. 58:299–327.

Pinault D, O'Brien TJ. 2005. Cellular and network mechanisms of genetically-determined absence seizures. Thalamus Relat Syst. 3:181–203.

Robinson RB, Siegelbaum SA. 2003. Hyperpolarization-activated cation currents: from molecules to physiological function. Annu Rev Physiol. 65:453–480.

Romanelli MN, Del Lungo M, Guandalini L, Zobeiri M, Gyökeres A, Árpádffy-Lovas T, Koncz I, Sartiani L, Bartolucci G, Dei S, et al. 2019. EC18 as a tool to understand the role of HCN4 channels in mediating hyperpolarization-activated current in tissues. ACS Med Chem Lett. doi:10.1021/acsmedchemlett. 8b00587.

Santoro B, Chen S, Lüthi A, Pavlidis P, Shumyatsky GP, Tibbs GR, Siegelbaum SA. 2000. Molecular and functional heterogeneity of hyperpolarization-activated pacemaker channels in the mouse CNS. J Neurosci. 20:5264–5275.

Santoro B, Lee JY, Englot DJ, Gildersleeve S, Piskorowski RA, Siegelbaum SA, Winawer MR, Blumenfeld H. 2010. Increased seizure severity and seizure-related death in mice lacking HCN1 channels. Epilepsia. 51:1624–1627.

Santoro B, Liu DT, Yao H, Bartsch D, Kandel ER, Siegelbaum SA, Tibbs GR. 1998. Identification of a gene encoding a hyperpolarization-activated pacemaker channel of brain. Cell. 93:717–729.

Sarnthein J, Jeanmonod D. 2008. High thalamocortical theta coherence in patients with neurogenic pain. Neuroimage. 39:1910–1917.

Sarnthein J, Morel A, von Stein A, Jeanmonod D. 2005. Thalamocortical theta coherence in neurological patients at rest and during a working memory task. Int J Psychophysiol. 57:87–96.

Schofield CM, Kleiman-Weiner M, Rudolph U, Huguenard JR. 2009. A gain in GABAA receptor synaptic strength in thalamus reduces oscillatory activity and absence seizures. Proc Natl Acad Sci USA. 106:7630–7635.

Schulman JJ, Cancro R, Lowe S, Lu F, Walton KD, Llinas RR. 2011. Imaging of thalamocortical dysrhythmia in neuropsychiatry. Front Hum Neurosci. 5:69.

Sherman SM, Guillery RW. 2006. Exploring the Thalamus and its Role in Cortical Function. Cambridge, London: The MIT Press.

Silbernagel N, Walecki M, Schafer MK, Kessler M, Zobeiri M, Rinne S, Kiper AK, Komadowski MA, Vowinkel KS, Wemhoner K, et al. 2018. The VAMP-associated protein VAPB is required for cardiac and neuronal pacemaker channel function. FASEB J. doi:10.1096/fj.201800246R.

Sitnikova E, van Luijtelaar G. 2006. Cortical and thalamic coherence during spike-wave seizures in WAG/Rij rats. Epilepsy Res. 71:159–180.

Stieber J, Herrmann S, Feil S, Loster J, Feil R, Biel M, Hofmann F, Ludwig A. 2003. The hyperpolarization-activated channel HCN4 is required for the generation of pacemaker action potentials in the embryonic heart. Proc Natl Acad Sci USA. 100:15235–15240.

Stieglitz MS, Fenske S, Hammelmann V, Becirovic E, Schottle V, Delorme JE, Scholl-Weidinger M, Mader R, Deussing J, Wolfer DP, et al. 2018. Disturbed processing of contextual information in HCN3 channel deficient mice. Front Mol Neurosci. 10:436.

Strauss U, Kole MH, Brauer AU, Pahnke J, Bajorat R, Rolfs A, Nitsch R, Deisz RA. 2004. An impaired neocortical Ih is associated with enhanced excitability and absence epilepsy. Eur J Neurosci. 19:3048–3058.

Talley EM, Solorzano G, Lei Q, Kim D, Bayliss DA. 2001. Cns distribution of members of the two-pore-domain (KCNK) potassium channel family. J Neurosci. 21:7491–7505.

Tronche F, Kellendonk C, Kretz O, Gass P, Anlag K, Orban PC, Bock R, Klein R, Schutz G. 1999. Disruption of the glucocorticoid receptor gene in the nervous system results in reduced anxiety. Nat Genet. 23:99–103.

van Luijtelaar EL, Coenen AM. 1986. Two types of electrocortical paroxysms in an inbred strain of rats. Neurosci Lett. 70: 393–397.

van Luijtelaar G, Sitnikova E. 2006. Global and focal aspects of absence epilepsy: the contribution of genetic models. Neurosci Biobehav Rev. 30:983–1003.

van Luijtelaar G, Wilde M, Citraro R, Scicchitano F, van Rijn C. 2012. Does antiepileptogenesis affect sleep in genetic epileptic rats? Int J Psychophysiol. 85:49–54.

van Luijtelaar G, Zobeiri M. 2014. Progress and outlooks in a genetic absence epilepsy model (WAG/Rij). Curr Med Chem. 21:704–721.

von Krosigk M, Bal T, McCormick DA. 1993. Cellular mechanisms of a synchronized oscillation in the thalamus. Science. 261:361–364.

von Krosigk M, Monckton JE, Reiner PB, McCormick DA. 1999. Dynamic properties of corticothalamic excitatory postsynaptic potentials and thalamic reticular inhibitory postsynaptic potentials in thalamocortical neurons of the guinea-pig dorsal lateral geniculate nucleus. Neuroscience. 91:7–20.

Wahl-Schott C, Biel M. 2009. HCN channels: structure, cellular regulation and physiological function. Cell Mol Life Sci. 66: 470–494.

Weiergraber M, Henry M, Hescheler J, Smyth N, Schneider T. 2005. Electrocorticographic and deep intracerebral EEG recording in mice using a telemetry system. Brain Res Brain Res Protoc. 14:154–164.

Wemhöner K, Kanyshkova T, Silbernagel N, Fernandez-Orth J, Bittner S, Kiper AK, Rinne S, Netter MF, Meuth SG, Budde T, et al. 2015. An N-terminal deletion variant of HCN1 in the epileptic WAG/Rij strain modulates HCN current densities. Front Mol Neurosci. 8:63.

Ying SW, Jia F, Abbas SY, Hofmann F, Ludwig A, Goldstein PA. 2007. Dendritic HCN2 channels constrain glutamate-driven excitability in reticular thalamic neurons. J Neurosci. 27: 8719–8732.

Yue BW, Huguenard JR. 2001. The role of H-current in regulating strength and frequency of thalamic network oscillations. Thalamus Relat Syst. 1:95–103.

Zhang Y, Llinas RR, Lisman JE. 2009. Inhibition of NMDARs in the nucleus reticularis of the thalamus produces delta frequency bursting. Front Neural Circuits. 3:20.

Zobeiri M, Chaudhary R, Datunashvili M, Heuermann RJ, Luttjohann A, Narayanan V, Balfanz S, Meuth P, Chetkovich DM, Pape HC, et al. 2018. Modulation of thalamocortical oscillations by TRIP8b, an auxiliary subunit for HCN channels. Brain Struct Funct. 223:1537–1564.

Zobeiri M, van Luijtelaar G, Budde T, Sysoev IV. 2018. The brain network in a model of thalamo-cortical dysrhythmia. Brain Connect. doi:10.1089/brain.2018.0621.